III International Conference on Particle-based Methods – Fundamentals and Applications
PARTICLES 2013
M. Bischoff, E. Oñate, D.R.J. Owen, E. Ramm & P. Wriggers (Eds)

FLUID-STRUCTURE INTERACTION WITH FLEXIBLE MULTIBODY DYNAMICS AND SMOOTHED PARTICLE HYDRODYNAMICS

M. Schörgenhumer[1], P. Seil[2], S. Pirker[3], and J. Gerstmayr[4]

[1,4] Austrian Center of Competence in Mechatronics GmbH (ACCM)
Altenberger Straße 69, 4040 Linz, Austria
{markus.schoergenhumer, johannes.gerstmayr}@accm.co.at, http://www.accm.co.at

Johannes Kepler University Linz
[2,3]Christian Doppler Laboratory of Particulate Flow Modelling
[3]Department of Particulate Flow Modelling
Altenberger Straße 69, 4040 Linz, Austria
{philippe.seil, stefan.pirker}@jku.at, http://www.jku.at/pfm

Key words: fluid-structure interaction, smoothed particle hydrodynamics, flexible multibody dynamics, Lattice Boltzmann, blood flow, flexible fibers

Abstract. In this work, we present a versatile and efficient computational approach to fluid-structure interaction based on the coupling of flexible multibody systems with fluids analyzed by means of the meshfree particle-based method smoothed particle hydrodynamics. Regarding numerical examples, rigid or flexible cells, and fibers in microchannel flows are investigated. As a main feature of this paper, our results are validated with reference simulations obtained from fundamentally different approaches.

1 INTRODUCTION

The numerical modelling of fluid-structure interaction (FSI, see, e.g., [1]) still is a challenging subject in both mechanics as well as fluid mechanics, and particularly difficult, if large displacements or deformation of the structural components are involved. In this work we present an approach to FSI which is based on the coupling of advanced methods from flexible multibody system dynamics with the meshfree method smoothed particle hydrodynamics (SPH, see e.g. [2]). The multibody formulation, on the one hand, allows for the static and dynamic simulation of very general mechanical systems involving rigid bodies, flexible components (classical finite elements and structural elements such as beams, plates, and shells), springs or actuators, as well as joints, constraints, and contact [3]. Particularly, the structural elements offer high efficiency and convergence order as well as a smooth geometric surface representation, even in case of highly non-linear problems with large deformation. The fluid dynamics, on the other hand, are computed using

the Navier-Stokes equations in SPH discretization and an interaction formalism based on distributed surface force fields for the fluid-structure contact [4]. The approach does not impose any fundamental restrictions with respect to geometry, motion or deformation of the mechanical components in contact with the fluid, and thus is aimed at both efficiency as well as applicability to a wide range of FSI problems in two or three dimensions, including free-surface flows due to the particle nature of SPH. An outline of the theoretical background and the coupling formalism is given in Sec. 2.

Regarding numerical examples, the focus is on the motion of rigid or flexible cells and highly deformable fibers in (micro)channel flows, which is an important subject in fields such as biomechanics (blood flow), microfluidics (cytometry, cell identification and separation), or industrial applications (e.g. production processes of fiber-reinforced materials) (cf. Sec. 3). Quantitative verification is provided via reference simulations by an immersed boundary Lattice Boltzmann implementation and the classical finite volume method for stationary cases.

2 THEORETICAL BACKGROUND

This section shall provide a brief overview of the underlying numerical models for the coupled simulation of the fluid and solid domain.

2.1 Multibody dynamics

The broad field of multibody dynamics is concerned with the static and dynamic analysis of so-called multibody systems, i.e., of general mechatronical systems consisting of mechanics, drives and embedded systems. The mechanical components, such as rigid or flexible bodies, can be mutually independent or interconnected with some kind of joint or constraint, and may undergo large translational and/or rotational motion, as well as deformation, being subject to external or internal forces, constraints, contact and friction, and, possibly, control.

The equations of motion of a multibody system can often be derived using Lagrange's equations of the first kind, along with a set of algebraic equations to account for constraints. For a system consisting of n_b bodies $i \in \{1, ..., n_b\}$ subject to n_c algebraic constraint equations $j \in \{1, ..., n_c\}$ those governing equations read, using the Einstein summation convention,

$$\begin{aligned} \frac{d}{dt}\left(\frac{\partial T^i}{\partial \dot{q}_k^i}\right) - \frac{\partial T^i}{\partial q_k^i} + \lambda_j \frac{\partial C_j}{\partial q_k^i} &= Q_k^i \qquad i \in \{1, ..., n_b\} \text{ and } k \in \{1, ..., n_f^i\} \\ C_j(\boldsymbol{q}^1, \boldsymbol{q}^2 ..., \boldsymbol{q}^{n_b}, t) &= 0 \qquad j \in \{1, ..., n_c\} \end{aligned} \tag{1}$$

in terms of the vector $\boldsymbol{q}^i$ of n_f^i generalized coordinates of each body i, where λ_j, $j \in \{1, ..., n_c\}$, are Lagrange multipliers [6]. T^i is the corresponding kinetic energy defined as

$$T^i = \frac{1}{2} \int_{V^i} \rho^i \dot{\boldsymbol{r}}^i \cdot \dot{\boldsymbol{r}}^i \, dV^i, \tag{2}$$

with the mass density ρ^i, the volume V^i, and the global coordinate vector $\boldsymbol{r}^i = \boldsymbol{r}^i(\boldsymbol{q}^i)$ of an arbitrary point P on the body. $\boldsymbol{Q}^i$ denotes the vector of generalized forces acting on body i, and can be computed using the principle of virtual work which states that, for any kinematically admissible virtual displacement $\delta\boldsymbol{q}^i$, the total work done by the constraint forces vanishes. Hence, the total virtual work δW is composed of the contributions $\delta W_{(s)}$ due to internal and $\delta W_{(e)}$ due to external forces, yielding

$$Q_k^i = \frac{\partial W}{\partial q_k^i} \quad \text{with} \quad \delta W = \delta W_{(s)} + \delta W_{(e)} = \sum_{i=1}^{n_b} \boldsymbol{Q}^i \cdot \delta\boldsymbol{q}^i \tag{3}$$

for the generalized forces.

The way how the generalized coordinates are chosen, and how the virtual work may be computed, depends on the properties of the respective bodies. In case of flexible bodies, $\boldsymbol{q}^i$ represents a set of nodal coordinates corresponding to the spatial discretization. Typical examples are classical continuum finite element formulations or structural finite elements, such as beams, plates, and shells. Some ways for the modelling of flexible bodies undergoing small or large deformations feature advantages over classical finite elements. We mention in particular the component mode synthesis, which aims to model deformations of complex geometries by means of a small set of reduced coordinates. With respect to fluid-structure interaction, the absolute nodal coordinate formulation is superior to classical large-deformation structural elements due to its ability to represent smooth surfaces of arbitrarily deformed beams or plates.

For further information regarding multibody dynamics in general see, for instance, the classic book of Shabana [6], for more specific topics refer to the respective literature.

2.2 Smoothed particle hydrodynamics

Smoothed particle hydrodynamics (SPH) is a meshfree particle-based Lagrangian method which was introduced into the field of fluid dynamics by Monaghan [7] in the 1990s. Over the years, it has been successfully applied to a wide range of flow problems, particularly to cases involving free surface flows and complex geometries; see [8] and the references therein for applications and some recent examples.

Assuming that the fluid domain is divided into small volume fractions represented by a set of $i \in \{1, ..., N\}$ discrete "particles" with associated positions $\boldsymbol{r}_i$, masses m_i, densities ρ_i, and corresponding volumes m_i/ρ_i, the so-called *particle approximation* of a field variable $g(\boldsymbol{r})$ – a sort of unstructured interpolation – is defined as [2]

$$g(\boldsymbol{r}) \approx \sum_{i=1}^{N} \frac{m_i}{\rho_i} g(\boldsymbol{r}_i) W(\boldsymbol{r} - \boldsymbol{r}_i, h), \tag{4}$$

with a suitable, compactly supported *smoothing kernel* $W(\boldsymbol{r}, \boldsymbol{r}', h)$, $W = 0$ if $|\boldsymbol{r} - \boldsymbol{r}'| > 2h$, and the *smoothing lenght* h. Hence, above sum effectively only runs over neighboring particles within the support domain of the kernel. Note that fluid here still is modelled

as a continuum, and therefore, the particles should not be confused with real physical particles, but rather be seen as the nodes of a spatial discretization.

The governing equations for isothermal compressible Newtonian fluids are given by the Navier-Stokes equations, i.e. the continuity and the momentum equation, along with a scalar equation of state, which, in Lagrangian form, can be discretized in terms of the SPH approximation (4) as

$$\begin{aligned} \frac{D\rho_i}{Dt} &= \sum_{j=1}^{N} m_j(\boldsymbol{v}_i - \boldsymbol{v}_j) \cdot \nabla_{\boldsymbol{r}_i} W(\boldsymbol{r}_i - \boldsymbol{r}_j, h) \\ \frac{D\boldsymbol{v}_i}{Dt} &= -\sum_{j=1}^{N} m_j \left(\frac{p_i}{\rho_i^2} + \frac{p_j}{\rho_j^2} + \Pi_{ij} \right) \cdot \nabla_{\boldsymbol{r}_i} W(\boldsymbol{r}_i - \boldsymbol{r}_j, h) + \boldsymbol{f}_i \\ p_i &= p(\rho_i), \end{aligned} \tag{5}$$

with the viscosity term

$$\Pi_{ij} = -\frac{16\mu}{\rho_0(\rho_i \rho_j)} \frac{(\boldsymbol{r}_i - \boldsymbol{r}_j) \cdot (\boldsymbol{v}_i - \boldsymbol{v}_j)}{(\boldsymbol{r}_i - \boldsymbol{r}_j)^2 + \eta^2} \tag{6}$$

for two dimensions, based on the well-known artificial viscosity by Monaghan [2]. Here, $\frac{D}{Dt}$ denotes the material time derivative, and the variables $\boldsymbol{r}_i$, $\boldsymbol{v}_i$, and $\boldsymbol{f}_i$ correspond to the position, velocity, and acceleration due to external forces of particle i; ρ_i and $p_i = p(\rho_i)$ designate the corresponding density and pressure, ρ_0 and μ are the fluids nominal density and dynamic viscosity, respectively, and $\eta \approx 0.01h$ is a parameter to improve numerical stability. In the present work we are using Tait's equation of state [7], and the 5th-order polynomial *Wendland* kernel [10]. Note that incompressible fluids here are modelled as weakly compressible.

More details on SPH can be found, for instance, in the book of Liu [9], or review papers such as [2, 9].

2.3 Coupling formalism

Concerning the coupling between the solid and the fluid domain, the following three points must be accounted for in FSI: Firstly, the fluid domain, in general, is time-dependent, and at least partially confined by the surfaces of each mechanical component in contact with the fluid. Secondly, for any viscous fluid, the *no-penetration* and *no-slip* condition must be fulfilled on any static or moving impervious boundary, i.e., the relative flow velocity must vanish on the boundary (*kinematic boundary condition*). Thirdly, the mechanical stress distribution on any boundary is given by the normal and shear forces due to the static pressure and viscous contributions of the fluid (*dynamic equilibrium*).

Several approaches have been developed for the implementation of boundaries in SPH, such as the generation of (virtual) boundary particles, kernel-adaption techniques, or force-field approaches (cf., e.g., [2, 7]). In the present work we follow an approach suggested in [11], and define over each boundary – no matter if a rigid wall or the surface

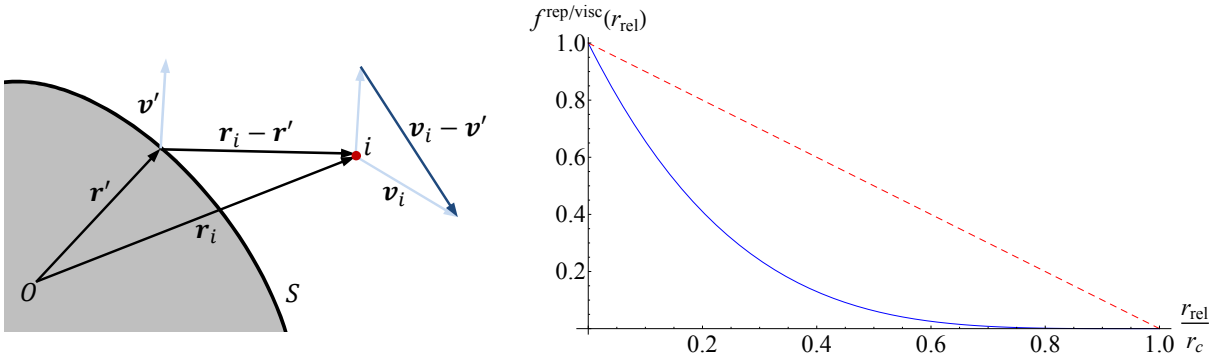

Figure 1: Left: Sketch of the interaction between a boundary S with SPH particle i (red dot); $\boldsymbol{r}'$ and $\boldsymbol{v}'$ denote position and velocity of a local point on the boundary, $\boldsymbol{r}_i$ and $\boldsymbol{v}_i$ of the SPH particle, respectively. Right: Plot of the absolute values of the normalized interaction force densities versus the normalized distance r_{rel}/r_c between an SPH particle and a local point on a boundary. The solid blue line represents the 4-th order repulsion term, while the dashed red line corresponds to the viscous contribution.

of a moving, deformable body – two short-ranged force field densities, a repulsive contribution $\boldsymbol{f}^{rep}$ to keep particles from penetrating the walls (no-penetration), and a viscous contribution $\boldsymbol{f}^{visc}$ to generate wall friction and enforce the no-slip condition. Based on that, the total forces $\boldsymbol{F}_i^{rep}$ and $\boldsymbol{F}_i^{visc}$ betweeen an SPH particle i and any boundary S – cf. the sketch in Fig. 1 – are defined by surface convolution integrals over the relative vectorial distance $\boldsymbol{r}_{rel} = \boldsymbol{r}_i - \boldsymbol{r}'$ and velocity $\boldsymbol{v}_{rel} = \boldsymbol{v}_i - \boldsymbol{v}'$ as

$$\boldsymbol{F}_i^{rep} = \int_S \boldsymbol{f}^{rep}(\boldsymbol{r}_{rel})\, dS' \quad \text{and} \quad \boldsymbol{F}_i^{visc} = \int_S \boldsymbol{f}^{visc}(\boldsymbol{r}_{rel}, \boldsymbol{v}_{rel})\, dS', \tag{7}$$

where $\boldsymbol{f}^{rep}$ and $\boldsymbol{f}^{visc}$ are given by

$$\boldsymbol{f}^{rep}(\boldsymbol{r}_{rel}) = k\left(1 - \frac{|\boldsymbol{r}_{rel}|}{r_c}\right)^4 \frac{\boldsymbol{r}_{rel}}{r_c} \quad \text{and} \quad \boldsymbol{f}^{visc}(\boldsymbol{r}_{rel}, \boldsymbol{v}_{rel}) = -t\boldsymbol{v}_{rel}\left(1 - \frac{\boldsymbol{r}_{rel}}{r_c}\right), \tag{8}$$

with the scaling parameters k and t, *if* the particle lies within the interaction range r_c, i.e., if $|\boldsymbol{r}_{rel}| < r_c$; otherwise, both force fields vanish. Of course, accounting for the dynamic equilibrium, the corresponding counterforces act on the component of the multibody system which is associated with S.

In our implementation, any boundary is associated with a surface mesh (line segments, or linear triangular elements for surfaces in 2D or 3D, respectively), in case of deformable objects defined in material coordinates of the undeformed reference configuration. Based on that, the integrals (7) then are computed numerically using Gauss-Legendre quadrature, resulting in a sum over discrete contributions each constituted by the pairwise interaction between one SPH particle and a local Gauss integration point on the discretized surface. Due to the short interaction range, which typically is chosen on the order of the SPH smoothing length, the spacing between the sampling points of the quadrature

rule must be sufficiently small in order to consistently represent a closed surface. To this end, the meshes are adaptively refined locally during the FSI force computation, i.e., any surface element is subdivided recursively until an appropriate resolution for the numerical integration has been reached.

See [4] for further details concerning the chosen potentials, the surface discretization and adaptive refinement, as well as the computation of the counterforces acting on the respective bodies.

2.4 Simulator coupling

In contrast to monolithic approaches, where the governing equations for the solid and the fluid part are solved fully coupled in one single system, our implementation is a so-called weakly-coupled partitioned scheme, based on the coupling of two simulation libraries: The multibody code "HOTINT" [3] is used for the simulation of the mechanical part, and calls an SPH implementation in "LIGGGHTS" [12], a parallel particle simulator, as external program for the computation of the fluid dynamics and the fluid-structure interaction in the sense of a co-simulation.

In short, in each time step HOTINT performs one implicit integration step of the multibody system, accounting for the current FSI forces, and then passes the updated geometry – positions and velocities of the nodes defining the surface meshes – to LIGGGHTS. The latter, in the mean time, has computed the first part of a timestep of the SPH simulation (fluid only, without FSI), and can now evaluate the fluid-structure contact based on the new boundary data, finally returning the new FSI forces to HOTINT.

Here, HOTINT plays the server role, and additionally is used for the setup, control, visualization during the computation, and post-processing of the coupled simulation. Note that, since both programs run on different platforms on different machines, communication and synchronization is done via TCP/IP. Further information again can be found in [4].

2.5 The Lattice Boltzmann method

The Lattice Boltzmann method (LB, LBM) [13] is a CFD method originating from lattice gas cellular automata. It uses a discretized version of Boltzmann's transport equation to compute fluid flows.

2.5.1 Basic LB

The LBM uses a set of discrete particle populations on each grid cell. Each of these populations represents a part of the fluid that is moving in a certain discrete direction. The evolution of these populations is governed by the LB equation

$$f_i\left(\boldsymbol{x}+\boldsymbol{c}_i, t+1\right) = f_i\left(\boldsymbol{x}, t\right) - \underbrace{\frac{1}{\tau}\left[f_i\left(\boldsymbol{x}, t\right) - f_i^{eq}\left(\rho, \boldsymbol{u}\right)\right]}_{\Omega_i^{BGK}} \tag{9}$$

where the Bhatnagar-Gross-Krook approximation for the collision term Ω_i^{BGK} is used [14]. It reflects the tendency towards an equilibrium distribution $f_i^{eq}(\rho, \boldsymbol{u})$, a second-order expansion of the Maxwell-Boltzmann distribution. $\tau = \frac{\nu}{c_s^2} - \frac{1}{2}$ is the dimensionless relaxation time. The vectors $\{\boldsymbol{c}_i\}$ are the discrete velocities and f_i can be understood as "the population that travels in direction $\boldsymbol{c}_i$". For the presented calculations, the D2Q9 scheme was used. It consists of the following nine velocities:

$$\boldsymbol{c}_0 = (0,0) \qquad \boldsymbol{c}_{1\ldots4} = (\pm1, 0), (0, \pm1) \qquad \boldsymbol{c}_{5\ldots8} = (\pm1, \pm1) \tag{10}$$

The macroscopic flow quantities can be computed from the populations via

$$\rho = \sum_i f_i \quad \text{and} \quad \boldsymbol{u}\rho = \sum_i f_i \boldsymbol{c}_i. \tag{11}$$

A Lattice Boltzmann timestep consists of two phases: Firstly, the populations of all cells are copied to their respective neighbors (*streaming*). Secondly, at each cell, the macroscopic flow quantities are computed following Eq. (11). Then, the populations are relaxed towards a local equilibrium by applying Ω^{BGK} (*collision*).

2.5.2 Immersed boundary LB

To couple the fluid calculations to a discrete phase, the method proposed by Noble and Torczinsky [15] was used. It is capable of handling partially filled cells and thus allows to model solid domains immersed in the flow by representing them as a solid fraction field. The modified LB equation reads

$$f_i(\boldsymbol{x} + \boldsymbol{c}_i, t+1) = f_i(\boldsymbol{x}, t) - (1 - \epsilon_s)\,\Omega_i^{BGK} + \epsilon_s \Omega_i^s, \tag{12}$$

where ϵ_s is the solid fraction in the cell. For the collision operator, the modification proposed by Holdych [16] was used,

$$\Omega_i^s = f_{-i}(\boldsymbol{x}, t) - f_{-i}^{eq}(\rho, \boldsymbol{u}_s) + f_i^{eq}(\rho, \boldsymbol{u}_s) - f_i(\boldsymbol{x}, t), \tag{13}$$

where $\boldsymbol{u}_s$ is the solid velocity. The force and torque on a body then can be evaluated from the collision operators via

$$\boldsymbol{F} = \sum_n B_s^n \sum_i \Omega_i^s \boldsymbol{c}_i \quad \text{and} \quad \boldsymbol{T} = \sum_n (\boldsymbol{x}_n - \boldsymbol{x}_0) \times \left(B_s^n \sum_i \Omega_i^s \boldsymbol{c}_i \right), \tag{14}$$

with $\sum_n$ reaching over all nodes covered by the body and $\boldsymbol{x}_0$ denoting its the center of mass.

2.5.3 Coupled calculations

As discussed in Subsec. 3.1, coupled calculations with one circular rigid cell in the simulation domain were performed. In the dynamic case, its trajectory was computed by numerical integration of Newton's law using the Velocity-Verlet algorithm.

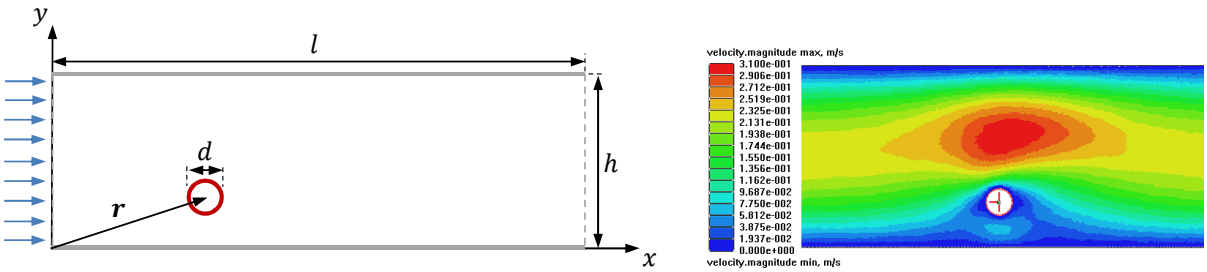

Figure 2: Left: Sketch of the test system: A circular cell (red) of diameter d is placed in a gravity-driven channel flow in x-direction, with periodic boundary conditions. The vector $\boldsymbol{r}$ designates the position of the cell center. Right: Snapshot of a coupled multibody dynamics - SPH simulation of the flow around a fixed rigid cell; the color map shows the absolute flow velocity.

3 NUMERICAL EXAMPLES AND VALIDATION

As already mentioned in the introduction, in the present work we have focussed on the quantitative investigation of rigid or deformable cells in microchannel flows (cf. Subsec. 3.1), and set up some test examples which involve fluid interaction with flexible fibers (see Subsec. 3.2).

3.1 Example 1: Cells in microchannel flows

The dynamic behavior of rigid or deformable cells in microchannel flows, such as white or red blood cells in microcapillares, is of interest in various scientific fields including biomechanics (blood flow) and microfluidics (cytometry, cell identification and cell separation) [18, 19].

As shown by the sketch in Fig. 2, here we consider a circular cell of diameter d and mass density $\rho_s = 1000\,\mathrm{kg/m^3}$ in a simple rectangular channel (length l, width b) with rigid walls parallel to the x-axis, filled with an incompressible fluid with a nominal mass density of $\rho_0 = 1000\,\mathrm{kg/m^3}$ and a dynamic viscosity of $\mu = 0.001\,\mathrm{Ns/m^2}$. At the walls and the surface of the cell, the no-slip condition holds, and at the channel in- and outlet periodic boundary conditions are applied. The flow is driven by gravity g in x-direction, which is computed from the analytic Poiseuille solution as

$$g = \frac{12\nu}{b^2}\bar{v}, \tag{15}$$

with the kinematic viscosity $\nu = \mu/\rho_0$, and the average in- or outlet flow velocity $\bar{v}$ of the undisturbed Poiseuille flow. No additional boundary condition, such as a Dirichlet condition for the pressure on the inlet, is specified and hence, the absolute value of the pressure remains undetermined. This, of course, should not affect the solution for incompressible flows.

Firstly, we have performed stationary benchmark computations in a channel with the dimensions $l = 250\,\mu\mathrm{m}$ and $b = 50\,\mu\mathrm{m}$, and an average Poiseuille velocity of $\bar{v} = 0.2\,\mathrm{m/s}$,

which corresponds to a Reynolds number of 10 with respect to the channel width. In case 1, the center of a rigid circular cell with $d = 8\,\mu$m was fixed at the position $\boldsymbol{r}_0 = (75\,\mu\text{m}, 25\,\mu\text{m})$, constrained to constant rotation about its center at an angular velocity of 62800 rad/s. In case 2, the cell was fixed at the point $\boldsymbol{r}_0 = (75\,\mu\text{m}, 12.5\,\mu\text{m})$, while its rotation was locked. For both cases, the drag force, lift force, and the torque on the cell were evaluated in the stationary state, with our coupled multibody dynamics - SPH approach (MBD-SPH), the immersed boundary Lattice Boltzmann code (IB-LB), and ANSYS Fluent as finite volume solver. As to the spatial resolution, approximately 90-100 cells or particles were used per channel width b in case of MBD-SPH and IB-LB, and a comparable resolution for the finite volume mesh. A comparison of the results is given in Table 1. We find a very satisfactory mutual agreement within a few percent for all cases and quantities, except for the lift force in case 1; the significant deviation of the MBD-SPH result here will be subject to future investigation. Secondly, we have

Table 1: Comparison of results for the drag force f_x in x-direction, the lift-force f_y in y-direction and the torque m acting on the cell for both stationary cases as discussed in the text, obtained from simulations using the finite volume solver ANSYS Fluent, the IB-LB implementation, and our coupled MBD-SPH approach.

	Case 1			Case 2		
	Fluent	**IB-LB**	**MBD-SPH**	**Fluent**	**IB-LB**	**MBD-SPH**
f_x $[10^{-3}\,\text{N}]$	2.60	2.64	2.70	2.11	2.13	2.22
f_y $[10^{-4}\,\text{N}]$	-7.62	-7.96	-5.40	4.60	4.68	4.32
m $[10^{-9}\,\text{Nm}]$	-12.92	-13.57	-12.55	-1.48	-1.54	-1.43

investigated various dynamic cases in which the cells are driven by the flow, starting from certain initial conditions. According to literature [18, 19], the cell approaches a lateral equilibrium position (in y-direction), which, in general, does not lie on the centerline of the channel. However, that position depends on the material properties of solid and fluid, the cells geometry and size (compared to the channel width), as well as the Reynolds number of the flow.

For a comparison between our approach and the IB-LB results, a rigid circular cell with $d = 8\,\mu$m was placed in a channel of width $b = 50\,\mu$m, with $\bar{v} = 2/3$m/s (Re = 50), at the initial position $\boldsymbol{r}_0 = (42.5\,\mu\text{m}, 6\,\mu\text{m})$ of the cell center and an initial velocity in x-direction equal to the velocity of the corresponding Poiseuille flow at that position. Furthermore, one test case simulated with our MBD-SPH formulation was added, where the rigid cell was replaced by a deformable one which was modelled based on a linear plate element, with the same circular shape in the undeformed reference configuration, and an elastic modulus and Poisson ratio of $33000\,\text{N/m}^2$ and 0.45, respectively. The same spatial resolution as for above stationary cases was used in all simulations.

The left-hand side of Fig. 3 summarizes our simulation results for the trajectory of the cell center in y-direction. We see very good agreement between the two computations

for the rigid cell, while keeping in mind that they have been performed with completely different methods. As expected, the flexible cell exhibits a different behavior, and moves towards another equilibrium position closer to the centerline of the channel while experiencing both rotation and shear deformation (cf. also the right-hand side of Fig. 3).

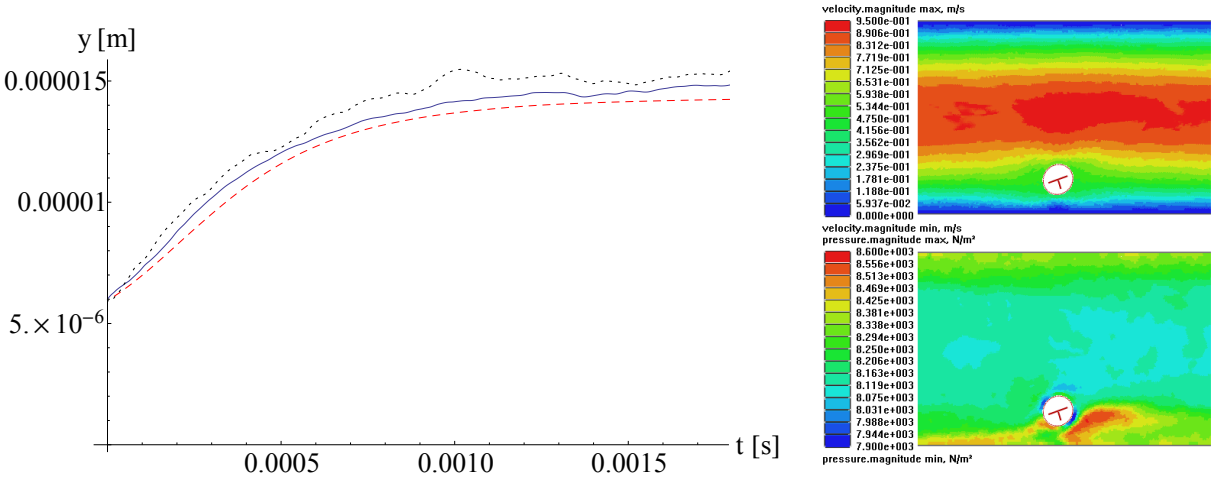

Figure 3: Left: Results for the trajectories of the cell in y-direction moving in the channel flow: The solid blue line and the dashed red line show the results for an identical simulation setup with a rigid circular cell (see text) simulated with our MBD-SPH approach and the IB-LB implementation, respectively. The dotted black line corresponds to a MBD-SPH computation where the rigid cell was replaced with a deformable one, modelled with a linear plate element. Right: Snapshot of a simulation with the flexible cell exhibiting shear deformation and rotation, shortly after the initial configuration. The contour plots show the absolute velocity and the pressure field, respectively.

3.2 Example 2: Flexible fibers with fluid interaction

Especially in the context of industrial processes such as the production of composite materials, the interaction of rigid or flexible fibers with fluids is an important aspect. Due to the efficient multibody formulation of various beam elements (cf. also Sec. 2.1), as well as the support of models for mechanical contact provided by HOTINT, the present approach is well suited for the investigation of such fiber-fluid interaction problems.

We have set up some test examples involving a set of fibers modelled by ANCF beam elements [17], including mutual mechanical contact as well as fiber-wall contact, which shall be presented here concludingly without any quantitative analysis. Fig. 4 shows one example of fibers moving in a channel flow (with periodic boundary conditions for the fluid) aroung a rigid, fixed obstacle, as well as a snapshot of a simulation where fibers immersed in a highly viscous fluid are injected into a mold by a piston pump. Here, the coupled fluid-fiber simulation helps to understand the fiber placement and orientation during an injection process.

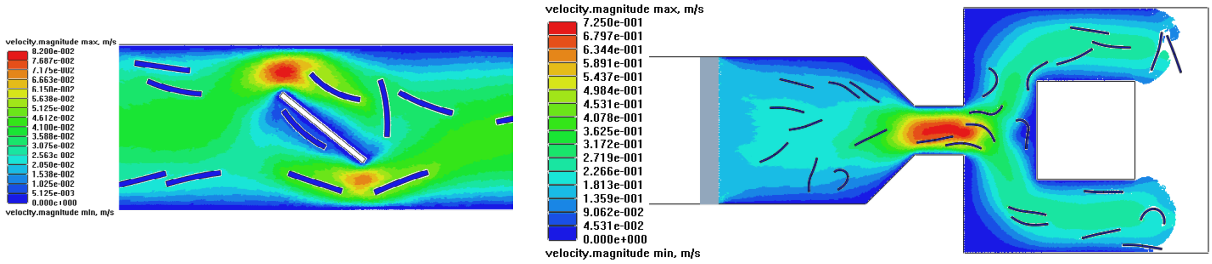

Figure 4: Left: Flexible fibers modelled by 2D ANCF beam elements [17] with fiber-fiber and fiber-wall contact in a channel flow (from left to right) around a rigid fixed obstacle (white bar). Right: Flexible fibers immersed in a highly viscous fluid during injection into a mold by a piston moving from left to right; note also the free fluid surface in the mold. In both plots, the color map corresponds to the absolute flow velocity.

4 OUTLOOK AND CONCLUSIONS

By direct coupling of flexible multibody systems with fluids modelled by means of SPH we have developed a versatile approach to FSI which, in the present work, was used for simulation of systems involving of rigid or flexible fibers or cells in microchannel flows. Validation of the method could be provided by satisfactory agreement with reference simulations based on fundamentally different, mesh-based approaches – an immersed boundary Lattice Boltzmann implementation, and the classical finite volume method.

5 ACKNOWLEDGEMENTS

The authors M. Schörgenhumer and J. Gerstmayr gratefully acknowledge the support of this work by the K2-Comet Austrian Center of Competence in Mechatronics (ACCM). Furthermore, they would like to thank P. Seil and S. Pirker for the fruitful collaboration.

REFERENCES

[1] Bungartz, H.J., Mehl, M., and Schäfer, M. (eds.) *Fluid-Structure Interaction II: Modelling, Simulation, Optimisation*. Springer, (2010).

[2] Monaghan, J.J. Smoothed particle hydrodynamics. *Rep. Prog. Phys.* (2005) **68**:1703–1759.

[3] Gerstmayr, J., et al. HOTINT - A Script Language Based Framework for the Simulation of Multibody Dynamics Systems. In: *Proceedings of the ASME 2013 IDETC/CIE*, Portland, OR, USA, (2013).
See also `www.hotint.org`

[4] Schörgenhumer, M., Gruber, P.G., Gerstmayr, J. Interaction of flexible multibody systems with fluids analyzed by means of smoothed particle hydrodynamics. *Multibody Syst. Dyn.* (2013) **30**:53–76.

[5] Seil, P., Pirker, S. Modelling lateral motion of finite-size buoyancy-free particles in shear flow. To be presented at the *DSFD 2013*, Yerevan, Armenia.

[6] Shabana, A.A. *Dynamics of Multibody Systems*. Third edition, Cambridge University Press, (2005).

[7] Monaghan, J.J. Simulating Free Surface Flows with SPH. *J. Comp. Phys.* (1994) **110**:399–406.

[8] Liu, M.B, Liu, G.R. Smoothed Particle Hydrodynamics (SPH): an Overview and Recent Developments. *Arch. Comput. Methods Eng.* (2010) **17**:25–76.

[9] Liu, G.R., Liu, M.B. *Smoothed Particle Hydrodynamics*. World Scientific Publishing, (2003).

[10] Macià, F., Antuono, M., Colagrossi, A., Souto-Iglesias, A. Benefits of using a Wendland kernel for free-surface flows. In: Rung, T., Ulrich, C. (eds.) *Proceedings of the 6th International SPHERIC Workshop*, Hamburg, Germany, (2010).

[11] Müller, M. et. al. Interaction of fluids with deformable solids. *Comp. Anim. Virtual Worlds* (2004) **15**:159–171.

[12] CFDEM - Open Source CFD, DEM, and CFD-DEM. `www.liggghts.com`, (5/2013).

[13] Mcnamara, G.R., Zanetti, G. Use of the Boltzmann equation to simulate lattice-gas automata. *Phys. Rev. Lett.* (1988) **61**:2332–2335.

[14] Bhatnagar, P.L., Gross E.P., Krook, M. A Model for Collision Processes in Gases. I. Small Amplitude Processes in Charged and Neutral One-Component Systems. *Phys. Rev.* (1954) **94**:511–525.

[15] Noble, D.R., Torczynski, J.R. A Lattice-Boltzmann Method for Partially Saturated Computational Cells. *Int. J. Mod. Phys. C* (1998) **09**:1189–1201.

[16] Holdych, D.J. *Lattice Boltzmann methods for diffuse and mobile interfaces*. PhD thesis, University of Illinois at Urbana, Champaign, (2003).

[17] Gerstmayr, J., Irschik, H. On the correct representation of bending and axial deformation in the absolute nodal coordinate formulation with an elastic line approach. *J. Sound Vib.* (2008) **318**:461–487.

[18] Lan, H., Khismatullin, D.B. A numerical study of the lateral migration and deformation of drops and leukocytes in a rectangular microchannel. *Int. J. Multiphase Flow* (2012) **47**:73–84.

[19] Shin, S.J., Sung, H.J. Dynamics of an elastic capsule in moderate Reynolds number Poiseuille flow. *Int. J. Heat Fluid Flow* (2012) **47**:25–36.